RESEARCH ARTICLE

Investigating the Role of Ag and Ga Content in the Stability of Wide-Gap (Ag,Cu)(In,Ga)Se$_2$ Thin-Film Solar Cells

Patrick Pearson,* Jan Keller, Lars Stolt, and Charlotte Platzer Björkman

The stability of thin-film solar cells spanning a wide range of compositions within the (Ag,Cu)(In,Ga)Se$_2$ material system is evaluated over time, after dry-heat annealing and after light soaking, and the role of Ag and Ga content is explored. Ag-free CuInSe$_2$ is relatively stable to annealing and storage, while Cu(In,Ga)Se$_2$ suffers a degradation of fill factor and carrier collection. High-Ga (Ag,Cu)(In,Ga) Se$_2$ suffers degradation of carrier collection after prolonged annealing, reducing the short-circuit current by $\approx$12%. Ga-free (Ag,Cu)InSe$_2$ loses up to a third of open-circuit voltage and a quarter of fill factor after all treatments are applied. All samples suffer voltage losses after light soaking, with the Ga-free devices losing up to 50 mV and those containing Ga losing up to 90 mV. Ag incorporation leads to a significant reduction in doping, and a significant increase in the response of doping to treatments, with the depletion width of (Ag,Cu)(In,Ga)Se$_2$ samples expanding from $\approx$0.1 μm as-grown to beyond 1.0 μm after all treatments, compared to the Cu(In,Ga)Se$_2$ sample variation of $\approx$0.1–0.3 μm. Connections between Ag content, doping instability, and performance degradation are discussed.

1. Introduction

It is well known that human society needs to shift to an electrified energy system powered by renewables. Photovoltaics will play a key role in this transition, with the increased flexibility (both figuratively and literally) of thin-film solar cells meaning that they are expected to expand their market share and feature prominently in sectors where silicon devices struggle, for example, building-integrated photovoltaics. There are many semiconductor materials with good light absorption properties that can be used to produce thin-film solar cells, with an established example

being Cu(In,Ga)Se$_2$ (CIGS). CIGS devices have reached record efficiencies (η) of 22.6%[1] and have a maximum theoretical efficiency of 33%.[2] It is widely believed that a new generation of multijunction, or more specifically tandem, devices will come to replace single-junction devices, due to their higher maximum efficiencies ($\approx$46%) and our growing energy needs.[3]

With a tunable bandgap of 1.0–1.7 eV (Ga-free to In-free), CIGS is well placed to be implemented as the top or bottom cell in a tandem device.[4] Unfortunately, it has been observed that as the Ga/(Ga+In) ratio (GGI) increases, the open-circuit voltage (V_{OC}) does not increase in line with the bandgap as might be expected, with an optimum GGI in the region of 0.25–0.30 (corresponding to a bandgap of $\approx$1.2 eV).[5–8] Potential causes for this include lattice distortion; an increase in the energetic depth and concentration of deep defects; detrimental Cu enrichment of the grain boundaries; and an unfavorable conduction band offset to the commonly used CdS buffer layer.[9–11] Partial substitution of Cu with Ag can improve the conduction band offset between high-Ga (Ag,Cu)(In,Ga)Se$_2$ (ACIGS) and CdS[12] and through a reduction in the alloy melting temperature, ease the growth of high-quality absorber material on transparent back contacts (common processing temperatures of $\approx$550° lead to harmful GaO$_x$ formation at the interface between CIGS and transparent conducting oxide [TCO] back contacts).[13–15]

Our group has investigated a large range of ACIGS compositions, primarily focusing on high-Ga, wide-gap material, yielding high V_{OC} and promising efficiencies.[16] In a previous work, we discovered that wide-gap ACIGS with bandgaps around 1.45 eV exhibit strong instabilities, with a significant dependence on group-I/group-III stoichiometry (I/III), linked to a strong dependence of net doping on I/III. The results of most significance were drastic short-circuit current (J_{SC}) losses after storage and a twenty-four hour anneal at 85 °C, as well as large V_{OC} losses after light soaking (LS).[17] The underlying mechanisms driving this instability are unclear, and we are now working to investigate different possible causes. In this work, the role of Ag and Ga content in the observed instabilities is explored, through the fabrication of samples spanning from Ag-free, Ga-free CuInSe$_2$ (CIS), to high-Ga ACIGS.

The device compositions were planned to cover the four corners of a compositional 'square' allowing the broad inspection of

P. Pearson, J. Keller, L. Stolt, C. Platzer Björkman
Division of Solar Cell Technology
Department of Material Science
Uppsala University
Box 534, 75121 Uppsala, Sweden
E-mail: patrick.pearson@angstrom.uu.se

The ORCID identification number(s) for the author(s) of this article can be found under https://doi.org/10.1002/pssb.202300170.

Table 1. Compositional range of full sample set in the investigation. AAC and GGI are constrained to a narrow range, with I/III spanning a region previously observed to exhibit high-treatment-induced response in ACIGS.[17] The column 'reference' gives the compositions of the representative samples presented in results, with the notation XX/YY/ZZ denoting the composition in the order (I/III)/GGI/AAC.

Sample	Composition				
	I/III	GGI	AAC	E_G [V]	Reference
CIS	$0.88 < 0.99$	0.00	0.00	0.97–1.00	0.88/0.02/0.01
CIGS	$0.82 < 0.92$	$0.73 < 0.76$	0.00	1.45–1.52	0.82/0.76/0.00
ACIS	$0.82 < 0.91$	0.00	$0.45 < 0.53$	1.04–1.05	0.84/0.00/0.45
ACIGS	$0.74 < 0.92$	$0.74 < 0.77$	$0.46 < 0.52$	1.47–1.48	0.86/0.76/0.49

the effects of Ga and Ag content on performance and stability (**Table 1**). In our previous work, a moderately off-stoichiometric region ($0.82 < I/III < 0.92$) was identified as highly responsive to treatments and we aimed to capture this region for comparison in this study.[17] The spread in GGI and Ag/(Ag+Cu) ratio (AAC) is kept narrow to enhance the comparability of different samples. Stability has been investigated by measuring samples on the day of fabrication; after 1 month; after a 1 h anneal at 85 °C, and after a 24 h hour anneal at 85 °C (see **Figure 1**). Annealing is performed in dry air and the devices are not encapsulated. A selection of samples from each material, spanning the I/III range, were light soaked for three hours under AM1.5 illumination using a Peltier element to limit sample heating (an increase of ≈10 °C was recorded over the 3 h). The effects of the stability treatments have been probed using current density–voltage (JV), external quantum efficiency (EQE), and capacitance-based measurements. It is important to highlight that the treatments were performed in sequence, without returning samples to an intermediate reference state. Indeed for (Ag,Cu)InSe$_2$ (ACIS) and ACIGS, it does not seem that it is possible to return doping (depletion) to an initial state, as will be shown below. The LS

treatments were performed approximately 3 weeks after the 24 h anneal; hence, pre-LS data is included in the figures to indicate any intermediate relaxation and give an accurate reference point against which to compare the LS state.

2. Results

2.1. Preassessment of the Effect of Absorber Stoichiometry

The results of this work will primarily be presented by highlighting trends from representative devices situated in the middle of the stoichiometric range and sharing similar AAC and GGI values, to allow for fair comparison. The compositions of these reference samples are given in Table 1. CIS and CIGS take the role as references against which to compare the behavior of ACIS and ACIGS. This approach is justified as we are primarily discussing the moderately off-stoichiometric 'active' region of $0.82 < I/III < 0.92$ and there is a good level of consistency in device performance in this region (see Figure S1–S4, Supporting Information). Overall, there is no apparent I/III dependence of EQE for CIS devices, and although close-stoichiometric CIGS devices exhibited better collection than moderately off-stoichiometric devices, the difference is small (see Figure S1 and S2, Supporting Information). Interestingly, close-stoichiometric (I/III≈0.91) ACIS devices were observed to be drastically different to moderately off-stoichiometric devices, with severely interface-limited EQE spectra and extreme voltage-dependent collection in the J–V curve, resulting in maximum V_{OC} of ≈100 meV and $\eta \leq 1.0\%$ (See Figure S5, Supporting Information). As a result, close-stoichiometric ACIS device data are not shown in sample-set figures. As observed in our previous work, close- and extremely off-stoichiometric ACIGS devices had (slightly) better EQE spectra than moderately off-stoichiometric devices, presumably due to stoichiometry-dependent doping (depletion width) variation.[17]

2.2. Stability Testing

As expected, consideration of EQE spectra confirms that high levels of Ga incorporation lead to a severely reduced bulk quality and a depletion-dependent collection profile (**Figure** 2b,d). Additionally, the incorporation of Ag leads to an improved long-wavelength collection (Figure 2c,d). Ga-free device spectra are seen to be highly stable. The ACIGS EQE spectrum is relatively stable with respect to storage and the 1 h anneal treatment, but exhibits significant degradation after the 24 h anneal with subsequent recovery following LS. The prolonged anneal-induced degradation and LS-induced recovery were observed in our previous work investigating the role of I/III on the stability of ACIGS; however, a 1 h anneal enhanced collection and a six month storage period severely degraded it (see Figure S6b, Supporting Information).[17] This difference in behavior with respect to the one hour anneal is unexpected and the single known difference between the sample sets is the Ag content, with $0.54 < AAC < 0.63$ in the previous work, representing an increase of ≈0.1 as compared to the values used in this work. It is difficult to evaluate the implications of the difference in response to long- and short-storage periods, as it has already been
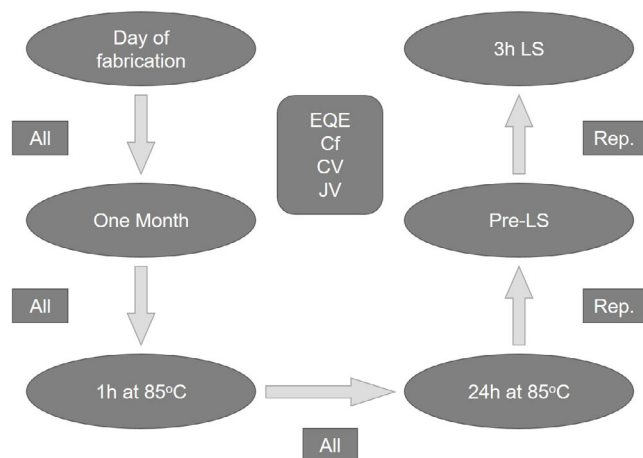

Figure 1. Treatment and measurement sequence for the sample set. All samples were characterized immediately after fabrication, after storage, and after two different annealing stages. A set of representative samples were further characterized before and after LS treatment.
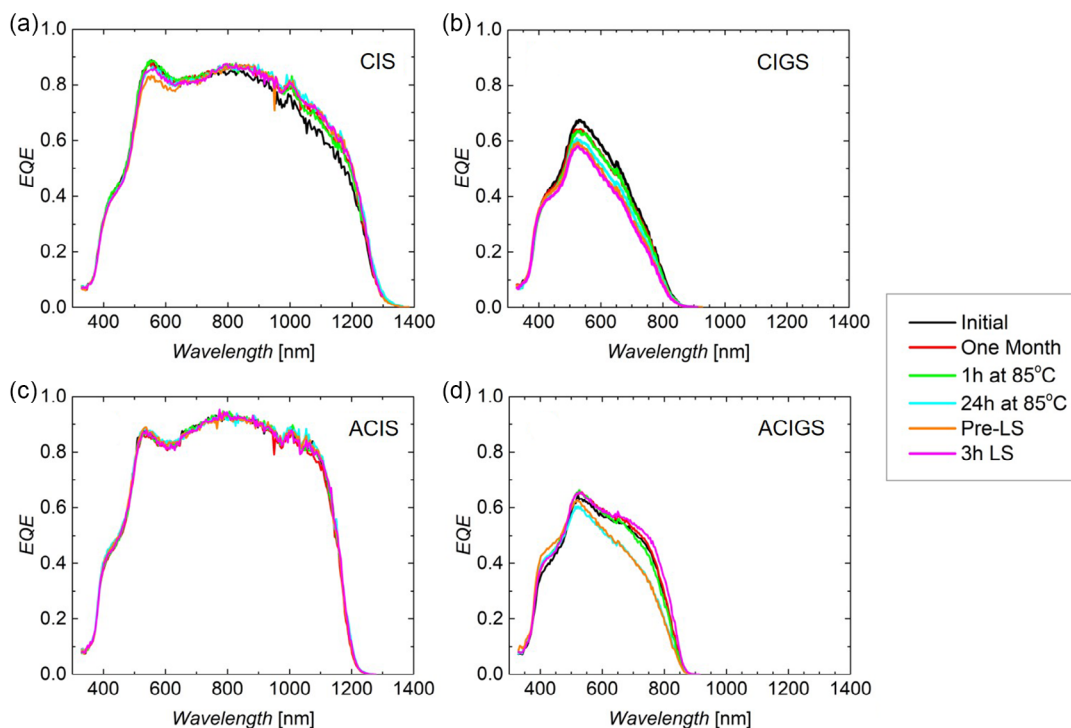
Figure 2. Evolution of EQE spectra of representative devices for each of the four materials, across all treatments. The high-Ga devices exhibit severe depletion-dependent collection (b,d), while the addition of Ag can be observed to improve long-wavelength carrier collection (c,d). Ga-free devices (a,c) show good collection and high stability.

seen that storage, short annealing, and prolonged annealing modulate doping in different ways, suggesting that there are multiple physical mechanisms operating on differing time scales.[17] It is possible that the differing lengths of the storage periods resulted in varying levels of oxygen- or humidity-induced degradation. Glow discharge optical spectroscopy (GDOES) spectra measured in the previous work, before and after annealing, revealed no measurable variation in oxygen content in the devices.[17] The devices analyzed in this study were only measured with GDOES on one occasion, but no difference in oxygen content was observed between the different materials (see Figure S8, Supporting Information). As such, we do not expect that oxygen- or humidity-induced degradation plays a significant role in the phenomena observed in this study, though some small effects cannot be ruled out.

Turning to J–V profiles, CIS is observed to have fairly good stability during storage and annealing, but develops a shunt slope as measurement progresses. The shunting may be linked to a high number of repeated measurements on nongridded cells, but it is also seen that there is a large reduction in the slope between the 24 h and pre-LS states, that is, a short storage period, indicating that the shunt could rather be induced by the treatments. The LS treatment induces losses in V_{OC} (30–60 mV) and a strong shunt slope, leading to a considerable reduction in η (1%–3% absolute, see **Figure 3**a). CIGS suffers from a gradual deterioration in both fill factor (FF) and J_{SC} (sample set averages reducing from $\approx$67% to 50% and from $\approx$12 to 10 mAcm^{-2}, respectively). Again, an LS-induced V_{OC} degradation is observed (55–95 mV); however, here there is no corresponding shunt,

indicating either a reduction in doping or increase in recombination induced by illumination (see Figure 3b). There is no indication of large bulk recombination increases in the EQE spectrum after LS, suggesting that this is not the cause (Figure 2b). ACIS devices exhibit much greater treatment-induced variations in performance parameters, with V_{OC} and FF both increasing substantially after the storage period (up to $\approx$100 mV and 10% absolute, respectively). Significant reductions in both parameters are induced during both the annealing stages and the LS treatment (post-LS sample set spread of 150–250 mV and 37–47%, compared to initial values of 250–350 mV and 47–57%, see Figure 3c). Again, there are no indications of large recombination from the EQE spectrum, which suggests that bulk recombination is not to blame for the V_{OC} reduction. ACIGS devices show greater stability to storage and 1 h annealing than the Ag-free samples, but suffer significant losses in J_{SC} ($\approx$2 mAcm^{-2} across the sample set) and FF (up to 5% absolute) induced by the 24 h anneal and significant V_{OC} losses induced by the LS treatment (up to 90 mV, see Figure 3d). This degradation of J_{SC} by the twenty-four hour anneal and the LS-induced degradation of V_{OC} were also observed in our previous work, with increasing V_{OC} losses for material toward the stoichiometric point, as is the case here (see Figure S4a, Supporting Information).[17] Unlike CIGS, ACIGS devices exhibit a slope around zero bias when illuminated, indicating strongly voltage-dependent collection. This is not unexpected, due to the clear impact of recombination losses on the EQE spectrum, but it is surprising that the CIGS devices do not display this property, despite the similarly recombination-limited EQE spectra.
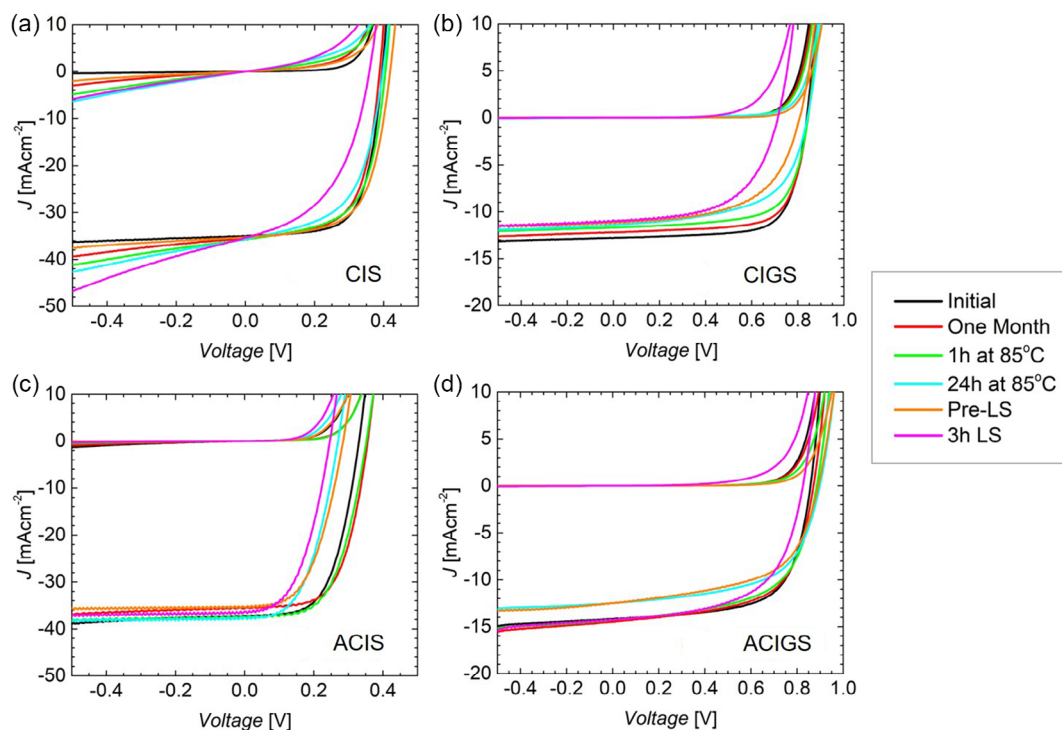
Figure 3. Evolution of dark and light J–V profiles for representative samples from each of the four materials, across all treatments. It can be observed that all samples suffer from significant LS-induced V_{OC} losses and that a) CIS is the most stable of the four materials; b) CIGS suffers continual degradation of FF and J_{SC} c) ACIS exhibits large variations in V_{OC} and FF; and d) ACIGS loses FF and J_{SC} after prolonged annealing.

A part of what has been observed in J–V and EQE measurements can be explained through consideration of the doping of the devices studied, a property tracked indirectly through the depletion width extracted at zero-bias from capacitance–voltage (C–V) measurements. Due to non-negligible hysteresis in CV measurements, the data points plotted here are extracted from single measurements performed at zero bias, as opposed to a full-voltage sweep, hence the notation 'ZP, Av' (sample average measured at the zero point). **Figure 4** shows the differences in forward and reverse CV sweeps for representative samples from each material. Although all samples exhibit some hysteresis, it was noted that ACIGS devices are the most affected (Figure 4d). Significant differences in capacitance recorded around the zero-bias point lead to large variations in the extracted depletion widths and net doping, with depletion width variations between forward and reverse sweeps of 20–120 nm across the sample set in the initial state (zero-point values of around 120 nm were measured for the most highly doped samples and 275–375 nm for the least doped). The most obvious cause of bias-dependent hysteresis is ion migration, with Na, Ag, and Cu are known to be highly mobile in the material.[18–21] However this would then lead one to expect a high degree of hysteresis behavior in ACIS, which is not observed (Figure 4c). It seems instead that it is the devices containing Ga that display the greatest hysteresis behavior (Figure 4b,c) indicating either that Ga significantly influences the ionic mobility of Cu, Na, and perhaps Ag and/or there is a significant electrostatic deep-state contribution to the CV measurement.[22]

Figure 5 maps the evolution of the sample-averaged depletion width of representative samples over the course of the stability treatments. It is immediately clear that CIS and CIGS have much more stable doping than their Ag-containing counterparts. Furthermore the Ag-free materials are much more highly doped (consider that the least doped CIS state is still more highly doped than the most highly doped ACIS state), though it can be noted that in the initial state, ACIGS has a similar level of doping to CIGS, depleting considerably after just one month in dark storage.

The doping of CIS and CIGS displays no dependence on I/III, within the explored region, as has been observed previously within a similar I/III region but for GGI $\approx 0.30, 0.45$.[23,24] The spread in I/III for ACIS is too narrow to evaluate, and ACIGS appears to initially match the trend we observed in our previous work, that is, a highly doped intermediate region for $0.82 < $ I/III $ < 0.92$ with an abrupt drop to almost full depletion for I/III ≈ 0.93 and a decrease in doping for more extremely off-stoichiometric material (**Figure 6**).[17,25] Another clear observation is that the initial doping state is never regained for the ACIGS and ACIS samples.

The doping of CIS and CIGS is slightly decreased by LS treatment, but not to such an extent that would explain the losses measured in V_{OC}. ACIS samples consistently gain in V_{OC} during the storage period (Figure 3c, **7**a). However both reductions and increases are observed in doping. The one hour anneal, however, has a clear connection between doping reduction and V_{OC} losses (Figure 7a); likewise, the 24 h anneal induces V_{OC} losses and
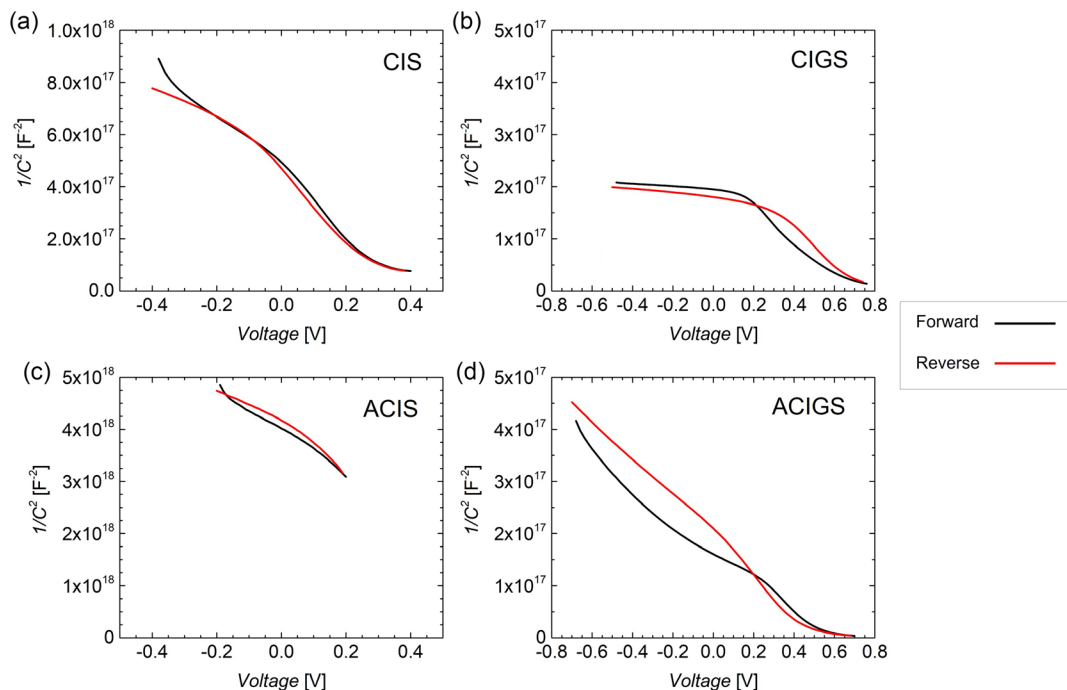
2300170 (4 of 9)

Figure 4. Inverse squared capacitance curves for representative samples for each of the four materials. All four devices display hysteresis to some degree, but the Ga-containing samples (b,d) exhibit greater effects, with the ACIGS being most severely affected (d). Note the differing scales for the Ga-free (a,c) and Ga-containing devices.
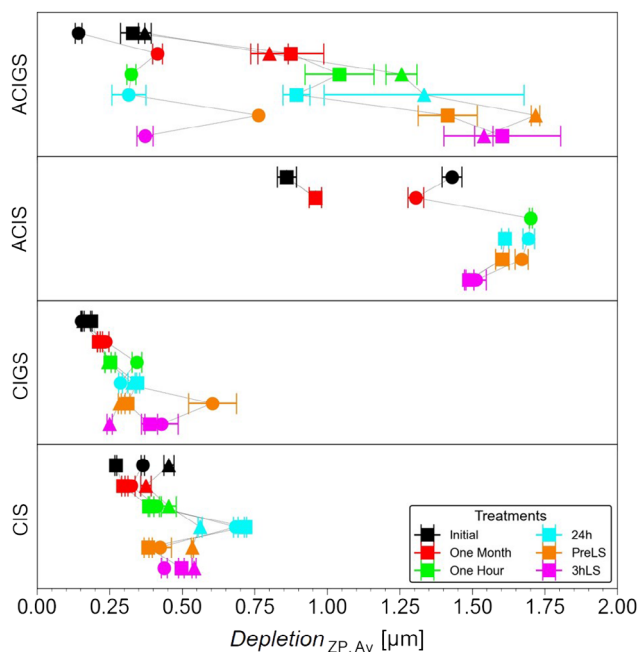

Figure 5. Evolution of depletion width measured at zero bias for representative samples from each material, averaged across three cells per sample, across all treatments. The connecting lines indicate the evolution path of individual samples. Note that one of the ACIS samples is missing data for the one hour anneal. The Ag-containing devices are typically much more depleted than their Ag-free counterparts and exhibit much greater treatment-induced variation in depletion width (doping) than the Ag-free devices.

either reduces doping or leaves it unchanged. The LS treatment also reduces V_{OC} but rather increases doping, which indicates that the variation is related to increased recombination losses, rather than a reduction of quasi-Fermi-level splitting. Overall, a strong connection can be seen between variations in depletion width and changes in V_{OC} for ACIS devices, a trend which is not shared with the other materials (Figure 7). For ACIGS, it would appear that the slight improvement in carrier collection after the one month dark storage is linked to reduction in doping and consequent expansion of the depletion region. It is, therefore, unexpected that the 24 h anneal, which causes a significant reduction in carrier collection and J_{SC} instead causes a doping reduction for many samples (Figure 5, 7b). A strong doping reduction is also observed in the pre-LS state of the ACIGS, presumably due to the same mechanism that leads to doping reductions in the initial storage period. Considering the magnitude of the changes in the net doping, it is surprising that carrier collection is not significantly modified, as the material has been estimated to have a poor diffusion length and displays clear recombination limited behavior in the EQE spectra (Figure 2).[17,25]

A final observation, which may also contain hints to explain the differences between Ag-free and Ag-containing samples, is determined from scanning electron microscopy (SEM) and GDOES. GDOES shows that Ag-containing samples have higher Na content than Ag-free samples (**Figure 8**a), with a particularly high level seen in ACIS. SEM images show that Ag incorporation significantly enhances grain size, which implies that the increased uptake of Na occurs in the grain interior, rather than boundaries (Figure 8b). This has previously been seen in a recent
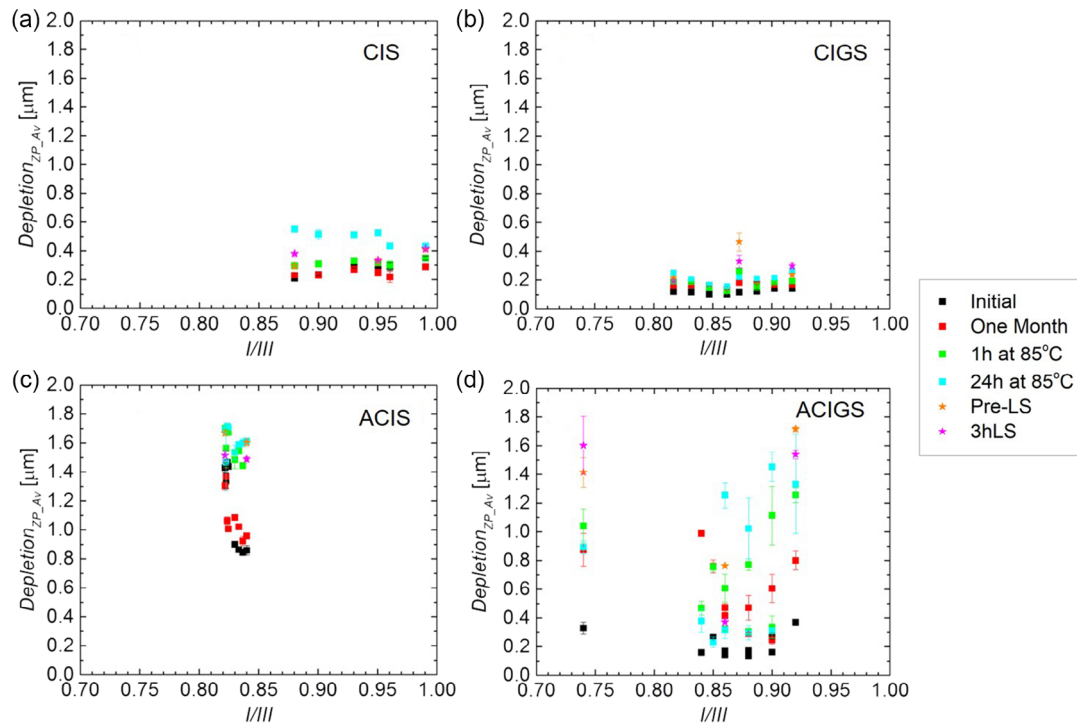
Figure 6. Depletion width measured at zero bias for the full sample set, averaged across three cells per sample, across all treatments. Ag-containing devices (c,d) exhibit much greater treatment-induced variation in depletion width (doping) than the Ag-free devices (a,b). The Ag-containing devices are typically much more depleted than their Ag-free counterparts.
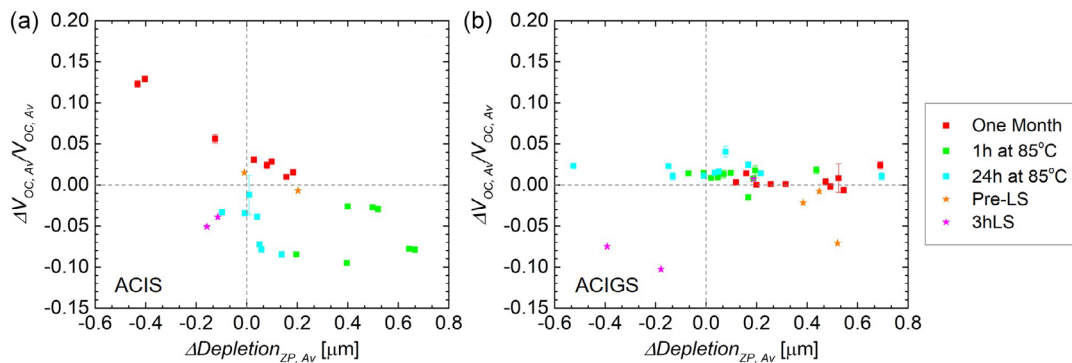

Figure 7. Evolution of the normalized change in V_{OC} due to treatment plotted against the corresponding change in depletion width for all ACIS (a) and ACIGS (b) samples. Measurement data is averaged across three cells per sample. A clear linear relationship between the V_{OC} change and depletion width expansion can be observed for the ACIS, but is absent for the ACIGS, which maintains a relatively uniform slight positive variation in V_{OC}, independent of depletion changes. Note that the legend in (b) applies also to (a).

work involving our group.[26] Another interesting feature is the clear shoulder near the front surface in the spectra of CIGS and ACIGS, which could be linked to the presence of ordered vacancy compounds (OVCs) at the (A)CIGS–CdS interface; as such OVCs are known to form with increasing frequency as off-stoichiometry increases and preferentially segregate Na in comparison to the 1:1:2 chalcopyrite phase.[27] The strong increase in Na at the rear of the devices is due to the Mo back contact which holds Na in the grain boundaries. GODES spectra showing all elements can be found in the supporting information, as can a wider scale SEM cross-section image.

3. Discussion

There are three clear statements regarding the impact of Ag incorporation in the CIGS material system that can be given from the observations we have made: Ag alloying leads to a significant reduction in the net doping of the material (ACIGS is initially only slightly less doped than CIGS on the day of fabrication but rapidly depletes in storage); Ag alloying leads to significant instabilities in the net doping of the material. Ag alloying promotes larger grain growth and an increased uptake of Na, both in the grain interiors and overall. The
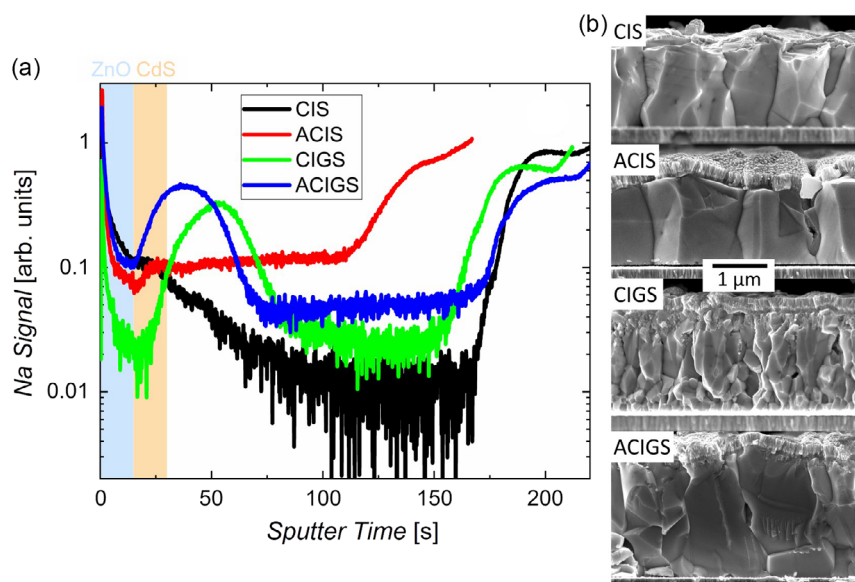
Figure 8. a) GDOES spectra tracking Na distribution in a representative sample of each of the four materials indicating a much higher level of Na incorporation in Ag-containing devices. b) SEM images of the same samples indicate that Na uptake is increased in grain interiors of the Ag-containing devices, as grain size is significantly increased in comparison to the Ag-free devices. The shaded blue and orange regions indicate the locations of the ZnO and CdS layers, respectively. The increase in Na signal at longer sputter times is due to the Mo rear contact being reached (Na is held in the grain boundaries).

reduction in net doping has been observed in previous studies[17,28,29] and has also been theoretically predicted for Cu-free $AgInSe_2$ and $AgGaSe_2$.[30] The theoretical explanation for reduced net doping is that in the Ag-poor growth regime, the formation energy of In/Ga_{Ag} defects (shallow donors) is lower than, or close to, that of V_{Ag} (shallow acceptors), indicating that the material could be intrinsic, or slightly n-type, if Ga-free, and intrinsic or slightly p-type for the In-free case, due to the very high levels of compensation. Thus the incorporation of Ag into p-type CIS and CIGS leads to a reduced p-type conductivity. A more phenomenological perspective is to consider that Ag alloying reduces the energetic height of the band edges, shifting the Fermi level away from the valence band and toward the midgap (with inferences from ref. [31]), or rather the valence band edge is shifted down with respect to the V_{Cu} defect state.

The instability of net doping is a concerning property and can lead to very significant changes in device performance, as observed for the ACIS samples presented here (Figure 7a) with a strong correlation between doping and V_{OC}. ACIGS samples in our previous work instead exhibited a strong dependence of J_{SC} on doping.[17] Variations that are seemingly uncorrelated with net doping have also been observed, for example, large losses in V_{OC} induced by LS treatments and degradation of FF following dark storage. It is also possible that there is a contribution from high-Ga contents (GGI > 0.50): There are several works exposing ACIGS with low-Ag content (AAC ≈ 0.2–0.3) and moderate-Ga content (GGI ≈ 0.3) to LS or annealing treatments, resulting in very similar behavior to CIGS with moderate-Ga content, that is, doping increases caused by LS, leading to improved V_{OC} and FF, reversible via dark annealing.[32,33] This is rather the opposite to what we see in this work with a GGI of ≈0.75. We have not

observed a direct dependence of doping variation on AAC; however, we do observe an increase in performance instability with increasing Ag content: In a previous work by our group, it was observed that after an 8 month storage period, ACIGS with GGI = 0.72 and AAC = 0.80 exhibited blocking behavior, consistent with the formation of a charge transport barrier,[27] whilst our previous study directly investigating stability indicated that ACIGS with a similar Ga content, but an AAC of ≈0.60, suffered significant degradation of carrier collection, but gave no evidence of blocking.[17] In turn this current study using a reduced AAC of ≈0.50 reveals a further reduced effect on device performance after storage and annealing.

It is also unclear how the increased Na content will affect device performance and whether it is connected to the reduced net doping and doping stability. The role of Na within CIGS is a heavily researched topic with several consistent observed effects of Na presence within devices. It is clear that Na is necessary for high-performance CIGS solar cells and that there is a connection between Na addition and net doping increase, and an improvement in carrier mobility, resulting in improved V_{OC} and FF.[34] It is also agreed that the majority of the Na within the device is segregated to the grain boundaries[35,36] and that there is a resulting reduction in recombination at the grain boundaries.[37] An increase in Na content has also been linked to an enhancement of the metastable net doping increase in Ag-free CIGS after LS treatment, though the mechanism for this is unknown.[38] In this work we see a decrease, rather than an increase, in net doping upon light soaking, and no evidence of improved FF between Ag-free and Ag-containing samples, despite the increased Na content of the latter. It has been reported that excess Na addition can be detrimental[39] and that the optimal Na content in

ACIGS is lower than that in CIGS. Indeed it is reported that the incorporation of K in ACIGS and ACIS can prove to be highly detrimental if not carefully managed, and can even reduce the net doping, despite its beneficial effect on CIGS.[40–42] Thus it may be possible that there is excessive Na incorporation in our Ag-containing devices, contributing in some way to their poor stability. Alternatively, there could be additional interactions between alkali metals and the ACIGS system, as compared to the CIGS system.

This work cannot unambiguously reveal the mechanisms controlling the variations in V_{OC}, J_{SC}, and FF. For ACIGS there are no strong variations in V_{OC} induced by storage and annealing, despite the large changes in net doping. Furthermore, it is seen that the doping increases, rather than decreases after illumination, despite an improvement in carrier collection (an apparent decrease in recombination) and strong decrease in V_{OC}. Surprisingly, the large changes in net doping are also not strongly correlated with variations in J_{SC}, despite the poor diffusion length of the material. ACIS exhibits a much closer relationship between V_{OC}, FF, and net doping, though there are several instances of counterintuitive increases (decreases) in doping corresponding to decreases (increases) in V_{OC}. In both cases it is clear that more commonly observed and predicted phenomena for low/moderate-Ga and low-Ag material are not being adhered to.

4. Conclusion

In this work the potential role of Ga and Ag content in the stability of devices within the $(Ag,Cu)(In,Ga)Se_2$ material system was investigated. We have shown that Ag incorporation leads to significant reduction in doping density and causes significant changes in net doping to be induced by storage and annealing treatments. An enhancement of carrier collection in the bulk is also observed for Ag-containing devices, presumably due to the increased depletion width resulting from the reduced doping. A third broad difference between Ag-free and Ag-incorporating devices is that Na incorporation is enhanced by Ag addition, seemingly within grain interiors due to a simultaneous increase in grain size. This increased level of Na could possibly affect the net doping and defect passivation in the material. In addition to doping instabilities, it was also shown that ACIS devices have highly variable FF and V_{OC}, which are significantly degraded by heating and illumination (approximate sample set reductions of 100 meV and 10% absolute, respectively). This material also shows a strong correlation between doping and V_{OC} variations, whilst the other three materials show no such coupling. Through comparing our current and previous works, we have concluded that an increased Ag content leads to much more severe degradation in ACIGS devices, for example, the formation of transport barriers and a stronger coupling of carrier collection and doping. A stable AAC region cannot be identified precisely; however, by reducing the AAC from ≈0.6 to ≈0.5, we have observed a reduction in the magnitude of degradation, while still retaining improved performance as compared to high-Ga CIGS. Additionally, it has also been suggested that an interplay between Ga and Ag exists, leading to the manifestation of differing stability phenomena, as can be seen through comparison of

ACIS and ACIGS devices, namely, the strong variation in V_{OC} that is observed only in the former, along with clear correlation of those V_{OC} changes with variations in net doping.

5. Experimental Section

The absorber layers of the devices were processed using the three-stage coevaporation process, with a maximum temperature of 550 °C. Chemical bath deposition was used for the CdS buffer layer and sputtering for the Mo back contact and TCO window stack. Devices were grown on a soda-lime glass substrate and completed with a ZnO:Al TCO layer, giving the following stack structure: $glass/Mo/(Ag,Cu)(In,Ga)Se_2/CdS/i-ZnO/ZnO$:Al. The process was not designed with the intention of deliberately providing a Ga grading throughout the device (i.e., constant In/Ga flux ratio), nor was an antireflective coating applied to the samples. Samples were divided into 28 cells, each of 0.05 cm^2. A total of 32 samples were characterized, six of CIS, eight each of CIGS and ACIS, and ten of ACIGS. Integral compositions were extracted from cross-calibrated X-ray fluorescence measurements on bare absorbers located at the outer positions of the deposition zone.

The characterization procedure was as follows: EQE measurement, capacitance–frequency profiling (admittance), capacitance–voltage profiling (C–V), and finally J–V measurements. This procedure was chosen as a result of previously observed voltage-dependent hysteresis and light-induced metastabilities, as well as the importance of net doping density as a tracking parameter for treatment effects.[17] EQE measurements are expected to cause minimal perturbation of the post-treatment state, as are admittance measurements with a small test voltage of 15 mV. CV measurements were measured first at zero bias, followed by forward and reverse sweeps at a test voltage frequency of 60 kHz, with a final zero bias measurement to evaluate voltage-induced changes. To avoid inaccuracies due to hysteresis behavior, we primarily utilize the zero-bias measurement to track material responses. The 60 kHz sweep frequency was chosen by considering the phase angle measured in admittance sweeps and by considering the presence of capacitance steps. This frequency was also used for the measurements in our previous work, allowing for direct comparison. A permittivity of 10 was used for all samples. The sweep voltage for CIS, CIGS, and ACIGS samples was varied over the range of $-0.5 < (V_{OC} - 0.1)$ V with ACIS samples being measured with a reduced range of $-0.2 < (V_{OC} - 0.05)$V, due to their low-voltage tolerance. J–V measurements were performed last, as illumination covered the entire sample, whilst the voltages applied in CV were confined to only those cells that were measured. J–V and EQE measurements were performed using home-built setups, the former used an ELH lamp for illumination and a water-cooled Peltier element to keep the cell temperatures at ≈25 °C. C–V measurements were performed with an Agilent 4284 A Precision LCR Meter and Keithley 2401 Source Meter. One sample for each of the four materials was measured with SEM and GDOES, utilizing a Zeiss Merlin instrument ($V_{acc} = 5$ kV) and Spectruma Analytik GDA 750 HR system, respectively.

Supporting Information

Supporting Information is available from the Wiley Online Library or from the author.

Conflict of Interest

The authors declare no conflict of interest.

Data Availability Statement

The data that support the findings of this study are available from the corresponding author upon reasonable request.

Keywords

[1] P. Jackson, R. Wuerz, D. Hariskos, E. Lotter, W. Witte, M. Powalla, *Phys. Status Solidi RRL* **2016**, *10*, 583.

[2] W. Shockley, H. J. Queisser, *J. Appl. Phys.* **1961**, *32*, 510.

[3] T. Leijtens, K. A. Bush, R. Prasanna, M. D. McGehee, *Nat. Energy* **2018**, *3*, 828.

[4] S. Wei, A. Zunger, *J. Appl. Phys.* **1995**, *78*, 3846.

[5] M. A. Contreras, L. M. Mansfield, B. Egaas, J. Li, M. Romero, R. Noufi, E. Rudiger-Voigt, W. Mannstadt, *Prog. Photovoltaics* **2012**, *20*, 843.

[6] P. T. Erslev, J. Lee, G. M. Hanket, W. N. Shafarman, J. D. Cohen, *Thin Solid Films* **2011**, *519*, 7296, proceedings of the EMRS 2010 Spring Meeting Symposium M: Thin Film Chalcogenide Photovoltaic Materials.

[7] A. Chikhalkar, M. Goryll, W. Shafarman, R. R. King, in *2019 IEEE 46th Photovoltaic Specialists Conf. (PVSC)*, IEEE, Piscataway, NJ **2019**, pp. 2150–2154.

[8] B. Huang, S. Chen, H. X. Deng, L. W. Wang, M. A. Contreras, R. Noufi, S. H. Wei, *IEEE J. Photovoltaics* **2014**, *4*, 477.

[9] G. Hanna, A. Jasenek, U. Rau, H. W. Schock, *Thin Solid Films* **2001**, *387*, 7173.

[10] J. V. Li, S. Grover, M. A. Contreras, K. Ramanathan, D. Kuciauskas, R. Noufi, *Sol. Energy Mater. Sol. Cells* **2014**, *124*, 143.

[11] M. Raghuwanshi, E. Cadel, P. Pareige, S. Duguay, F. Couzinie-Devy, L. Arzel, N. Barreau, *Appl. Phys. Lett.* **2014**, *105*, 013902.

[12] J. Keller, K. V. Sopiha, O. Stolt, L. Stolt, C. Persson, J. J. Scragg, T. Törndahl, M. Edoff, *Prog. Photovoltaics* **2020**, *28*, 237.

[13] S. C. Yang, T. Y. Lin, M. Ochoa, H. Lai, R. Kothandaraman, F. Fu, A. N. Tiwari, R. Carron, *Nat. Energy* **2023**, *8*, 40.

[14] C. Wang, D. Zhuang, M. Zhao, Y. Li, L. Dong, H. Wang, J. Wei, Q. Gong, *J. Energy Chem.* **2022**, *66*, 218.

[15] W. Shafarman, C. Thompson, J. Boyle, G. Hanket, P. Erslev, J. David Cohen, in *2010 35th IEEE Photovoltaic Specialists Conf.*, IEEE, Piscataway, NJ **2010**, pp. 000325–000329.

[16] J. Keller, H. Aboulfadl, L. Stolt, O. Donzel-Gargand, M. Edoff, *Sol. RRL* **2022**, *6*, 2200044.

[17] P. Pearson, J. Keller, L. Stolt, M. Edoff, C. Platzer Björkman, *Phys. Status Solidi B* **2022**, *259*, 2200104.

[18] G. Dagan, T. F. Ciszek, D. Cahen, *Fluid Phase Equilib.* **1992**, *96*, 3013.

[19] V. Fjallstrom, P. M. Salome, A. Hultqvist, M. Edoff, T. Jarmar, B. G. Aitken, K. Zhang, K. Fuller, C. K. Williams, *IEEE J. Photovoltaics* **2013**, *3*, 1090.

[20] J. F. Guillemoles, L. Kronik, D. Cahen, U. Rau, A. Jasenek, H. W. Schock, *J. Phys. Chem. B* **2000**, *104*, 4849.

[21] M. Theelen, N. Barreau, V. Hans, H. Steijvers, Z. Vroon, M. Zeman, in *2015 IEEE 42nd Photovoltaic Specialist Conf. (PVSC)*, IEEE, Piscataway, NJ **2015**, https://doi.org/10.1109/PVSC.2015.7355776.

[22] P. K. Paul, J. Bailey, G. Zapalac, A. R. Arehart, in *2017 IEEE 44th Photovoltaic Specialist Conference (PVSC)* **2017**, pp. 2414–2418.

[23] E. Avancini, R. Carron, B. Bissig, P. Reinhard, R. Menozzi, G. Sozzi, S. Di Napoli, T. Feurer, S. Nishiwaki, S. Buecheler, A. N. Tiwari, *Prog. Photovoltaics: Res. Appl.* **2017**, *25*, 233.

[24] T. Nakada, H. Ohbo, M. Fukuda, A. Kunioka, *Sol. Energy Mater. Sol. Cells* **1997**, *49*, 261.

[25] J. Keller, P. Pearson, N. Shariati Nilsson, O. Stolt, L. Stolt, M. Edoff, *Sol. RRL* **2021**, *5*, 2100403.

[26] H. Aboulfadl, K. V. Sopiha, J. Keller, J. K. Larsen, J. J. Scragg, C. Persson, M. Thuvander, M. Edoff, *ACS Appl. Mater. Interfaces* **2021**, *13*, 7188.

[27] J. Keller, L. Stolt, K. V. Sopiha, J. K. Larsen, L. Riekehr, M. Edoff, *Sol. RRL* **2020**, *4*, 2000508.

[28] A. Kanevce, S. Essig, S. Paetel, W. Hempel, D. Hariskos, T. M. Friedlmeier, *EPJ Photovoltaics* **2022**, *13*, 28.

[29] N. Valdes, J. Lee, W. Shafarman, *Sol. Energy Mater. Sol. Cells* **2019**, *195*, 155.

[30] R. Wang, B. Dou, Y. Zheng, S.-H. Wei, *Sci. China Phys., Mech. Astron.* **2022**, *65*, 107311.

[31] A. Goyal, P. Gorai, S. Anand, E. S. Toberer, G. J. Snyder, V. Stevanović, *Chem. Mater.* **2020**, *32*, 4467.

[32] P. Erslev, G. M. Hanket, W. N. Shafarman, D. J. Cohen, *MRS Proc.* **2009**, *1165*, 1165.

[33] A. J. Ferguson, R. Farshchi, P. K. Paul, P. Dippo, J. Bailey, D. Poplavskyy, A. Khanam, F. Tuomisto, A. R. Arehart, D. Kuciauskas, *J. Appl. Phys.* **2020**, *127*, 215702.

[34] A. Czudek, A. Eslam, A. Urbaniak, P. Zabierowski, R. Wuerz, M. Igalson, *J. Appl. Phys.* **2020**, *128*, 173102.

[35] M. Raghuwanshi, E. Cadel, S. Duguay, L. Arzel, N. Barreau, P. Pareige, *Prog. Photovoltaics: Res. Appl.* **2017**, *25*, 367.

[36] M. Raghuwanshi, R. Wuerz, O. Cojocaru-Mirédin, *Adv. Funct. Mater.* **2020**, *30*, 2001046.

[37] G. Sozzi, O. Cojocaru-Mirédin, R. Wuerz, In *2021 IEEE 48th Photovoltaic Specialists Conf. (PVSC)*, IEEE, Piscataway, NJ **2021**, pp. 0187–0191.

[38] A. Czudek, A. Urbaniak, A. Eslam, R. Wuerz, M. Igalson, *IEEE J. Photovoltaics* **2020**, *10*, 1926.

[39] R. Caballero, C. A. Kaufmann, T. Eisenbarth, T. Unold, R. Klenk, H.-W. Schock, *Prog. Photovoltaics: Res. Appl.* **2011**, *19*, 547.

[40] N. H. Valdes, J. Lee, W. N. Shafarman, *IEEE J. Photovoltaics* **2019**, *9*, 906.

[41] O. Donzel-Gargand, F. Larsson, T. Törndahl, L. Stolt, M. Edoff, *Prog. Photovoltaics: Res. Appl.* **2019**, *27*, 220.

[42] N. H. Valdes, K. J. Jones, R. L. Opila, W. N. Shafarman, *IEEE J. Photovoltaics* **2019**, *9*, 1846.